Multifractal spectrum observed in the Universe distribution of galaxies

Cite as: Chaos 36, 023129 (2026); doi: 10.1063/5.0289242
Submitted: 6 July 2025 · Accepted: 11 January 2026 ·
Published Online: 18 February 2026

W. M. Macek[a),b)] and D. Wójcik[c)]

AFFILIATIONS

Space Research Centre, Polish Academy of Sciences, Bartycka 18A, 00-716 Warsaw, Poland

[a)]**Also at:** Institute of Physical Sciences, Faculty of Mathematics and Natural Sciences, Cardinal Stefan Wyszyński University, Wóycickiego 1/3, 01-938 Warsaw, Poland. **Electronic mail:** macek@uksw.edu.pl
[b)]**Author to whom correspondence should be addressed:** macek@cbk.waw.pl. **URL:** http://www.cbk.waw.pl/~macek
[c)]**Electronic mail:** dwojcik@cbk.waw.pl

ABSTRACT

Nature's fractal patterns should, in theory, exhibit some common characteristics as revealed by a number of space missions carried out in the neighborhood of Earth's space environment. Here, we show that the overall shape of the multifractal spectrum of galaxies resembles that of NASA's Voyager mission observed at the heliospheric boundaries. We have, therefore, employed the same method—grounded on well-known results from up to one million galaxies in the updated redshift database—to identify a reliable multifractal spectrum of the distribution of galaxies on cosmological scales. We show that the observed spectrum fits the weighted Cantor set, which serves as a template for the turbulence observed in the heliosphere. In the universe, this would be indicative of the galaxy distribution's nonlinear multifractal scaling. For galaxies receding from the Sun at different distances, the degree of multifractality somewhat varies but is smaller than that inside the heliosphere. This could be connected to the presence of voids in the large-scale distribution of matter. Some variations from the Hubble law for the ideal uniform expansion might explain a possible asymmetry of the spectrum. We anticipate that finding nonlinear fractal scaling laws of galaxies will be a major step toward the ultimate explanation of the matter distribution in the Universe, especially fitting on the hundredth anniversary of discovery of the first galaxy beyond the Milky Way.

This study examines if the fractal scaling laws discovered with the multifractal analysis is offering a plausible explanation of galaxies in the visible Universe's distribution. We demonstrate that the observed multifractal spectrum is mostly in line with the weighted Cantor model that is characteristic for laboratory and space turbulence. The universal multifractal function for galaxies is similar to that discovered by NASA's Voyager missions in the outer heliosphere and even at the heliopause, the outermost heliospheric boundary, but with smaller degree of multifractality, even though the underlying physical processes are different.

I. INTRODUCTION

In the eighteen century, Immanuel Kant suggested that some nebulae might be distant systems of stars, but the first galaxy beyond the Milky Way Galaxy was discovered only in 1924. In fact, by the early twentieth century, based on observations using 2.5-m and 5-m telescopes on Mount Wilson and Palmer Mountain, respectively, Edwin Hubble has established the view the expanding Universe with galaxies receding from the Solar System, with velocities roughly proportional to their celestial distances. At present, after the past one hundred years, one can estimate that even a trillion of galaxies, $(0.2 - 2) \times 10^{12}$, may exist in the entire Universe. Because of, e.g., the problem of dark matter raised nearly half a century ago, not all the galaxies can admittedly be observed directly, but some fractions of them are now classified and well cataloged. Anyway, this allows us to study in more detail the large-scale structure of the distribution of galaxies in the Universe.

Incidentally, if the infinite Euclidean three-dimensional space ($D = 3$) had been filled-up with uniformly distributed celestial bodies and a constant density of mass distribution, this would have led to the sky lit always near uniformly; this Blazing Sky effect is often called Olbers's paradox. Aside with the Newtonian gravitational

force exerting on the object (immersed in an infinite gravitational potential) would also been infinite (p. 92 of Ref. 1). Admittedly, this paradox could be eliminated by relativistic theory and the expanding Universe. Therefore, despite the discovery of large massive inhomogeneous structures with large spatial empty voids, which are common features of astrophysical observations, the standard cosmological model based on the theory of general relativity also employs a somewhat similar approximation claiming that the Universe is homogeneous, at least on some very large scales.

However, since the galaxies are actually clustered, the expansion of the Universe is basically compatible not only with standard homogeneity but also with *fractal* homogeneity in a hierarchical fractal cosmology, as postulated by Mandelbrot (Chap. 32 of Ref. 1). Further, the available data satisfy power law distributions of mass with various exponents that are substantially lower than three, ranging from a value greater than 1 to about 2, see part III of his seminal book.[1] This would correspond to special values of various fractal dimensions, $D < 3$, see the monograph (Chap. 3.3 of Ref. 2 and Chap. 4 of Ref. 3). Naturally, this fractal approach does not depend on cosmological models resulting from general relativity, but would allow for a night dark sky for any scenario of the evolution of the Universe. Therefore, in this paper, we intend to investigate as to whether the fractal scaling laws identified now with the multifractal analysis provide a reasonable explanation of galaxy distribution in the visible Universe.

By the way, we have recently argued that a simple nonlinear law could possibly be important for the origin of the Universe resulting in fractal or multifractal features (Chap. 3.4 of Ref. 2, Chap. 4 of Ref. 3). According to the standard model of the evolution of the Universe, the first stars and galaxies appeared 200 or 400 millions years after the Big Bang, i.e., much later than the microwave background light was emitted (400 thousand years). Apparently, the conditions of these earlier times are imprinted on this light and could possibly forms a backlight for later development of the Universe. But to find a direct connection between background fluctuations and the currently observed fractal scaling laws is still far beyond the scope of the current study. Anyway, the fractal view of galaxy clusters is supported by luminous radiation data and is consistent with a flat Universe in thermodynamic equilibrium; in addition, this certainly satisfies the Copernican principle.

Some simple monofractal distributions of galaxies have been reported in the astrophysical literature,[4,5] including a correlation dimension calculated to probe homogeneity in the local universe.[6] But, it seems that the clustering structures with number $N(l)$ at distance l are better explained by the multifractal spectrum of dimensions $f(\alpha)$ with $N(l) \propto l^{-f(\alpha)}$.[7,8] The richness of various fractal scaling behavior has been exploited in Ref. 9. Interestingly, the universal multifractal function for galaxies is similar to that identified using magnetic field data collected by NASA's Voyager missions in the outer heliosphere[10–12] and even at the heliospheric boundaries, upon entering the very local interstellar medium for the first time in human history.[13] Obviously, cosmological scale are much larger than those in the space near the Solar System. However, the multifractal spectrum should exhibit some universal properties,[14] we therefore apply the similar fractal numerical methods here for direct determination of the multifractal spectrum of distribution of galaxies on cosmological scales, using the best currently available catalog.[15] We show that the observed multifractal spectrum is basically consistent with a one-scale Cantor model characteristic for turbulence in space and laboratory.[13,16,17]

In Sec. II, a concise description of the best currently available Updated Redshift Catalog (*UZCAT*) of the observed galaxies is provided, while Sec. III (with the multifractal model in SubSec. III B) outlines modern tools of multifractal analysis. The vital results of our analysis are presented in Sec. IV, which demonstrates that the solutions of the weighted Cantor models are in good agreement with the observed multifractal spectrum in the distribution of galaxies. Finally, Sec. V emphasizes the significance of the identified fractal scaling laws which could be an important contribution toward ultimate explanations of the distribution of matter in the visible Universe.

II. GALACTIC DATA

We have used in our analysis the data of redshifts obtained from the Smithsonian Astronomical Observatory Telescope Data Center available from http://tdc-www.harvard.edu/zcat/velocity.dat.[40] Instead of the older *CfA* catalog with only 359 objects and the apparent magnitudes $m \leq 14.5$, as analyzed in Ref. 18, we have now looked at the Updated (June 2008) CfA Redshift (Z)CATalog *UZCAT* compilation of a million (from a trillion) of various observed galaxies, see http://tdc-www.harvard.edu/zcat/zcom.htm.[41] This catalog originally consisted of various sets of galaxies (e.g., NZ40, SDSS, 2dF, 6dF, and ZCAT), and later other published observed data on some galaxies has been added by the catalogue authors, e.g.,[19–21] *ZBIG* for higher ($>100\,000\,\mathrm{km\,s^{-1}}$) relativistic velocities.[22] However, we have not used velocities with negative source designations (19 517 observations), which are in private domain (and hence cannot be used without the owner's consent).

After all, the data assembled by various authors for studying the large-scale structure of the Universe are basically complete in redshift information, but not necessarily in some other terms like diameter, magnitude, and references. As it is known in statistics data completeness is a measure of how much essential information is included in a data set or a model, and describes whether there are any gaps, missing values, or biases introduced impacting the results. This property is obviously important, as analysis on incomplete data is not meaningful, and the results may be questionable. It can be tested in various ways, for instance calculating the percentage of completeness for individual subsets and the entire data set, or visualizing the distribution and structure of missing data and testing/comparing distributions. In our case, however, for individual smaller sets the percentage of completeness is around 90%–99%, which is certainly well acceptable, with the lowest completeness in CfA survey which is only 80%. For the whole set, which is arguably large, we have systematically used a random data sampling method to estimate completeness, and the results were very similar.

Hence, the velocities based on the redshift data are the best available with respect to the quoted measurement errors and the reliability of the source. Surely, the purpose of this catalog is to be a complete list of galaxies with radial velocities for mapping and statistical studies. Incidentally, following remark that users should remove objects of type > 20, which were misclassified as galaxies, before using this galaxy catalog, 14 177 observations of V_H have been

omitted. The most frequent type was 25—a plate flaw, stars, and other misclassifications.

We have used here the radial velocities $V_H(r) < c$, with light speed $c = 299\,792\,458\,\mathrm{m\,s^{-1}}$, for a casting cosmological relativistic redshift $z = \sqrt{\frac{1+V_H/c}{1-V_H/c}} - 1$, see e.g.,[23] which in a nonrelativistic limit of $V_H \ll c$ is $z \approx V_H/c$, can somewhat be corrected for the motion of the Sun, with the apex velocity of $\sim 230\,\mathrm{km\,s^{-1}}$, right ascension (RA) 18 h 28 m and declination (Dec.) +30 deg (North in galactic coordinates). Therefore, we have, cf. 22,

$$V_H = \begin{cases} c\,z & \text{for } V_H \ll c, \\ c\,\dfrac{(1+z)^2 - 1}{(1+z)^2 + 1} & \text{otherwise,} \end{cases} \tag{1}$$

and the heliocentric distance to any galaxy is given by $L_H := \frac{c}{H_0} \ln(1+z) = \frac{c}{2H_0} \ln \frac{1+V_H/c}{1-V_H/c}$, and for $z \ll 1$ is $L_H \approx \frac{cz}{H_0}$, or $L_H \approx V_H/H_0$, assuming a Hubble parameter (present epoch) $H_0 = 70\,\mathrm{km\,s^{-1}\,Mpc^{-1}}$.

Strictly speaking, we have gotten rid of negative (blushifted) redshifts z, eliminated data gaps ($\sim$50 000 blank velocities), and removed outliers using the IQR method, which is useful for skewed data (in contrast to the usual Z-score method), i.e., $\mathrm{IQR} = Q_3 - Q_1$, where $Q_{1,3}$ are the first and third quartiles correspondingly, and then the outliers are defined as observations falling below $Q_1 - 1.5\,\mathrm{IQR}$, or above $Q_1 + 1.5\,\mathrm{IQR}$. Thus, we have analyzed the sample of 783 152 observations down to magnitude $m \lesssim 29.5$ (as limited by the Hubble Space Telescope) and moderate relativistic velocities up to $V_H/c \approx 0.72$, corresponding to $z \approx 1.46$). After all, one can confirm that for the currently estimated diameter of the Universe of about $2R_{max} \approx 28.5\,\mathrm{Gpc}$, the maximum receding velocity in most remote galaxies in the last category denoted by violet should be $V_{\max} = c\tanh(2R_{\max}H_0/c) = 293\,018\,\mathrm{km\,s^{-1}}$ (with $V_H/c = 0.98$ and a very large redshift $z_{\max} = 8.35$).

The plot of the distribution on the sky of the selected galaxies of *UZCAT* (Aitoff projection) is illustrated in Fig. 1, for the following various categories of nearby and more and more distant remote galaxies: red, blue, magenta, cyan, green, orange, and violet. We have used here right ascension and declination in the Galactic (J2000) coordinate system (centered at 0° increasing to the left). In particular, the green and orange groups represent the well studied regions of the 2dF GRS (initially 100 000, up to 380 000 datapoints) http://www.2dfgrs.net. The SDSS DR3 Survey https://classic.sdss.org/dr3/[24] consists of $\sim$350 000 galaxies and then we also have the LCRS and the Century surveys, as extensively studied by John Huchra and Zwicky. The clusters rely on published finding charts, and these clusters are standardized by ID's using Dressler's numbers.[25]

Apparently, the observable universe, with possible hundreds billion large galaxies, is not randomly distributed. The galaxies form intricate filaments and other large structures, shaping a web-like pattern that defines the large-scale structure of the cosmos. This pattern

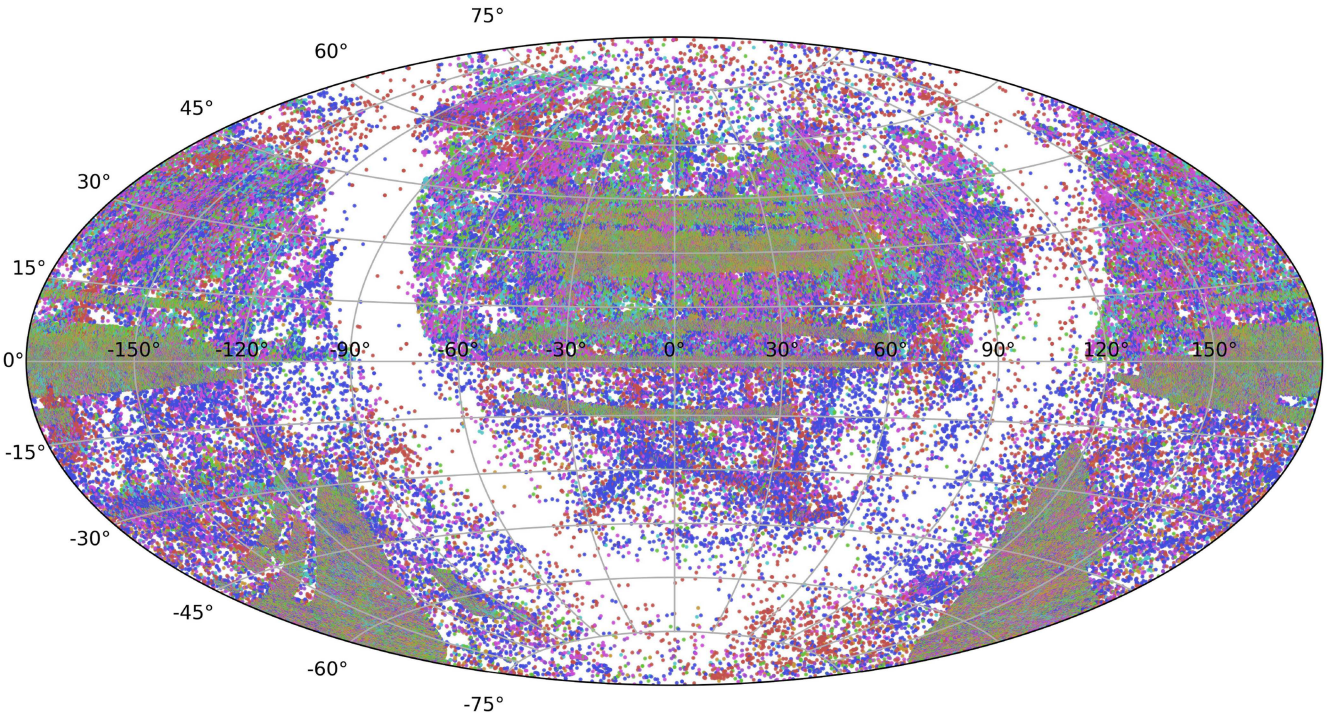

FIG. 1. The sky map of the distribution of different categories of galaxies: red, blue, magenta, cyan, green, orange, and violet depending of the receding speed using the UZCAT updated (2008) catalog with populations displayed in Table I.

TABLE I. Values of parameters describing multifractality Δ and asymmetry A of the spectra for the redshifts from the *UZCAT* catalog (with their calculated respective standard deviations) for variously populated categories of distances to remote galaxies (in 10^3 km s^{-1}).

Galactic category	Velocity max	Redshift max	Population $\mathcal{N}$	Multifractality $\Delta\,(\pm\sigma_\Delta)$	Asymmetry $A\,(\pm\sigma_A)$
Red	5	0.0168	21 556	0.0862 ± 0.0023	0.8817 ± 0.1015
Blue	12	0.0409	77 026	0.0822 ± 0.0013	0.9677 ± 0.1084
Magenta	20	0.0667	115 233	0.1225 ± 0.0023	1.0884 ± 0.1537
Cyan	25	0.0871	85 905	0.0855 ± 0.0026	1.1093 ± 0.1536
Green	40	0.1434	203 561	0.0873 ± 0.0013	0.7793 ± 0.1002
Orange	80	0.3214	192 982	0.1087 ± 0.0018	1.4238 ± 0.0704
Violet	≤ 215	1.4565	86 820	0.1687 ± 0.0019	1.2244 ± 0.0354
Total			783 152	0.1631 ± 0.0022	0.8369 ± 0.0611

reflects the behavior of dark matter and provides insights into the Universe's overall structure and evolution. Obviously, differences in population of each category of galaxies could result in specific somewhat different fractal and multifractal characteristics. Using statistical tests, such as MCAR (Missing Completely at Random), MAR (Missing at Random), and MNAR (Missing Not at Random) tests, we have verified that a small incompleteness of the redshift data used in our analysis does not changes the obtained results listed in Table I.

In Fig. 2, the box plot of various populations for the following categories of the galaxies under study: red, blue, magenta, cyan, green, orange, and violet is displayed depending on the receding speed together with the empirical probability density functions (PDFs), which have been computed using kernel density estimates (KDEs). All the KDE plots show generally low densities across different ranges. They exhibit minor but no dominant peaks, indicating a multimodal distribution with several small clusters. The data points appear to be spread out evenly across the ranges, with no significant concentration. The skewness is well pronounced in the contrasting cases.

III. FRACTAL ANALYSIS

The basic concepts of fractal sets are elucidated in standard textbooks.[14,26] We only note here that a fractal with the usual measure of the volume of the set is characterized by self-similarity, which is described by a single fractal dimension, as discussed in Chap. 3 of Ref. 14. On the other hand, a multifractal is a more complex object with a probability measure to visit a fraction of the set (Chap. 9 of Ref. 14). It can therefore be regarded, in a rough sense, as an interwoven family of fractals of different singularity strengths α, whose relative weights are quantified by the multifractal singularity spectrum $f(\alpha)$, see Ref. 27. In particular, its maximum value is simply the box counting (capacity) dimension. This universal properly has been tested experimentally for the plethora of systems, also in space.[11–13,28]

A. Nonlinear fractal characteristics

A comparison of the main characteristics of fractals (with a usual measure of the volume of a set) and multifractals (with a probability measure to visit a fraction of the set) has been thoroughly discussed in Sec. 1 of Ref. 13.

As is known, contrary to ordinary monofractal scaling, basically two universal functions are characteristic for multifractals. Namely, for a set consisting of N elements with probability measures $p_i(l)$ associated with a given scale l, the generalized dimension is [see Eq. (3.14) in Ref. 14]

$$D_q = \frac{1}{q-1}\lim_{l\to 0}\frac{\log\sum_{i=1}^{N}(p_i)^q}{\log l}, \tag{2}$$

while the multifractal singularity spectrum $f(\alpha)$ as a function of the singularity strength α [where $p_i(l) \propto l^{\alpha_i}$] is defined by [Eq. (17.4) of Ref. 26]

$$f(\alpha) = \lim_{\varepsilon\to 0}\lim_{l\to 0}\frac{\log[N_l(\alpha+\varepsilon) - N_l(\alpha-\varepsilon)]}{\log 1/l}. \tag{3}$$

In general, the generalized dimensions D_q are nonlinear functions of any given real index q and provide important information about multifractality of the system, see Sec. 3.3 of Ref. 14. Equivalently, the universal singularity spectrum $f(\alpha)$, with the maximum value at the box-counting dimension $f(\alpha_0) = D_0 = \lim_{l\to 0}\log N/\log l$, characterize multifractality of the system under study.[26] The line joining the origin to the point of the information dimension $f(D_1) = D_1 = \lim_{l\to 0}\sum_{i=1}^{N}[p_i(l)\log(p_i(l)]/\log(l)$ is tangent to the shape of the spectrum. It is worth noting that the generalized dimension D_q, which is a non-increasing function of q, and the concave down shape of $f(\alpha)$ as a function of singularity strength α tend to exhibit a similar form across a variety of physical systems, as illustrated in Fig. 9.1 of Ref. 14, cf. Fig. 3.7 of Ref. 2. These functions, as thoroughly discussed in Refs. 11 and 12, allow a comparison of the experimental results with the phenomenological models of turbulence.[29,30]

In addition to a usual probability measure $p_i(l)$, we can also use the following higher-order pseudoprobability measures associated with each scale l:

$$\mu_i(q,l) \equiv \frac{p_i^q(l)}{\sum_{i=1}^{N} p_i^q(l)}. \tag{4}$$

In this way (using a fractal dimension index $f_i(q,l) \equiv \log\mu_i(q,l)/\log l$), one can directly calculate the multifractal spectrum as the average of the pseudoprobability measure $\mu_i(q,l)$ according to

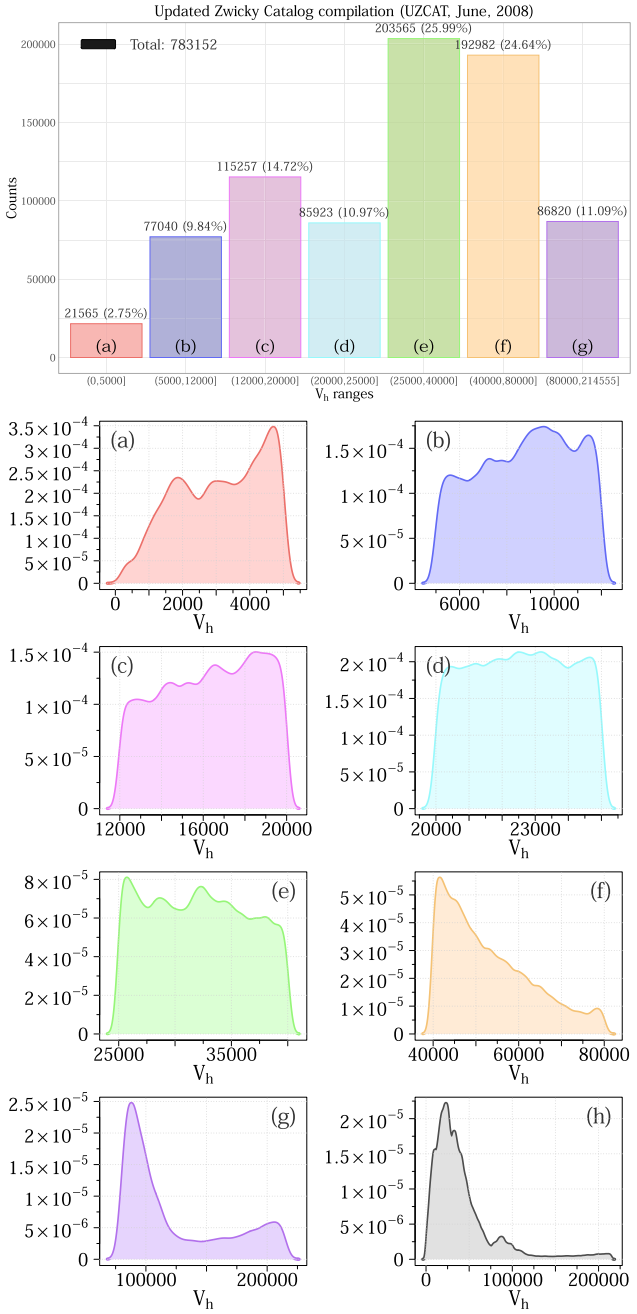

FIG. 2. The box plot of distribution and probability density functions (PDFs) of different colored categories of galaxies red, blue, magenta, cyan, green, orange, and violet depending of the receding speed of the UZCAT updated (2008) catalog with populations displayed in Table I.

Eq. (4) indicated by the squared brackets $\langle\cdots\rangle$,[31]

$$f(q) \equiv \lim_{l\to 0}\sum_{i=1}^{N}\mu_i(q,l)\,f_i(q,l) = \lim_{l\to 0}\frac{\langle\log\mu_i(q,l)\rangle}{\log(l)}. \tag{5}$$

The average value of the singularity strength is given by[32]

$$\alpha(q) \equiv \lim_{l\to 0}\sum_{i=1}^{N}\mu_i(q,l)\,\alpha_i(l) = \lim_{l\to 0}\frac{\langle\log p_i(l)\rangle}{\log(l)}. \tag{6}$$

B. Multifractal model

We have already argued that simple nonlinear or fractal models provides a useful tool for phenomenological analysis of complex turbulent media.[3,13] For example, the generalized weighted Cantor set is a simple example of multifractals, as explained, e.g., in the textbook.[26] This model is illustrated in Fig. 2 of Ref. 33. When constructing this model with one-scale parameter $l_1 = l_2 := \lambda \le 1/2$, we have the analytical expressions for D_q and $f(\alpha)$.[28] Namely, if measures p and $1-p$ are applied to the left and right remaining parts of a unit interval, the function $\tau(q) \equiv (q-1)D_q$ is given by Eq. (11) in Ref. 12

$$\tau(q) = \frac{\log[p^q + (1-p)^q]}{\log\lambda}, \tag{7}$$

and for $\alpha(q) = \tau'(q)$, we have the following formula:

$$\alpha(q) = \frac{1}{\log\lambda}\,\frac{p^q\log p + (1-p)^q\log(1-p)}{p^q + (1-p)^q}. \tag{8}$$

Then, using the Legendre transformation, we obtain the explicit formula for the multifractal spectrum $f(\alpha(q)) = q\alpha(q) - \tau(q)$.

However, for a more developed generalized two-scale weighted Cantor set, we must specify two scales l_1 and l_2 ($l_1 \neq l_2$), satisfying $l_1 + l_2 \le 1$. In this case, one needs to solve for $\tau(q)$ the transcendental equation, e.g.,[14]

$$\frac{p_1^q}{l_1^{\tau(q)}} + \frac{p_2^q}{l_2^{\tau(q)}} = 1, \tag{9}$$

which is only somewhat more general than the analytical solution given by Eq. (7). Finally, it is worth to mention that the standard middle-thirds monofractal Cantor set model is recovered only for $\lambda = 1/3$ and $p = 1/2$, with $D_0 = \log 2/\log 3$.

The difference between the calculated maximum and minimum dimensions, related to the respective regions in the phase space with the least and most dense probability densities, has been proposed in Refs. 28 and 33,

$$\Delta \equiv \alpha_{\max} - \alpha_{\min} = D_{-\infty} - D_{\infty} = \left|\frac{\log(1-p)}{\log l_2} - \frac{\log(p)}{\log l_1}\right|, \tag{10}$$

as a degree of multifractality. Naturally, this parameter Δ exhibits a deviation from a strict monofractal self-similarity, and it can also be used as a degree of intermittency as explained in (Chap. 8 of Ref. 29). The next quantitative parameter, describing the multifractal scaling, is the measure of asymmetry of the spectrum defined[28]

$$A \equiv \frac{\alpha_0 - \alpha_{\min}}{\alpha_{\max} - \alpha_0}, \tag{11}$$

where $\alpha = \alpha_0$ is the point at which the spectrum has its maximum, $f(\alpha_0) = D_0$. The case when $A = 1$ ($l_1 = l_2 = 1/2$) corresponds to the one-scale p-model.[34]

Now, following Ref. 35, the probability measures $p(l)$ depending on scale $l := L_H$, as discussed in Sec. II, can be constructed

using observed distribution of galaxies. First normalizing the series of average numbers of the observed objects $n(l_i)$ in the ith shell of radius l_i, where $i = 1, \ldots, \mathcal{N} = 2^m$ (e.g., taking $m = 17$) for $j = 2^{m-k}$, $k = 0, 1, \ldots, m$, one defines

$$p(x_j, l) \equiv \frac{1}{\mathcal{N}} \sum_{i=1+(j-1)\Delta l}^{j\Delta l} n(l_i) = p_j(l), \tag{12}$$

where the successive average values $\langle n(l_i + \Delta l)\rangle$ are taken over the intervals between $n(l_i)$ and $l_i + \Delta l$, for each $\Delta l = 2^k$ with the total $\mathcal{N}$ number of galaxies in the system.[11]

One can show that in the inertial range of scales the average value of the qth moment of p at various scales l should scale as[35]

$$\langle p^q(l)\rangle \sim l^{\gamma(q)}, \tag{13}$$

where the exponent γ is related to the generalized dimension, $\gamma(q) = (q-1)(D_q - 1)$. Using this method, the values of D_q can be determined from the slopes of $\log p_q(l)$ vs $\log l$ for each real q, according to Eq. (13). Alternatively, the multifractal function $f(\alpha)$ vs scaling index α, which exhibits universality of the multifractal scaling behavior, can be obtained using the Legendre transformation. It is worth noting, however, that we obtain this multifractal universal function directly from the slopes given in Eqs. (5) and (6), using this direct method in various situations.[11–13,28]

IV. RESULTS

Admittedly, with the *CfA* limited observations, one can only determine the points near the maximum of $f(\alpha)$.[18] One can perhaps extrapolate these points toward the intercepts at the maximum, where $f(\alpha_0) = D_0$. On the other hand, in our study, based on much more extensive *UZCAT* data of redshifted distances presented in Sec. II, Eq. (1), and using fractal methods described in Sec. III A, with the multifractal model of Sec. III B, we can now derive a more reliable multifractal spectrum for the distribution of galaxies in the Universe.

Therefore, we consider astronomical surveys at different right ascension (RA) and declination (Dec) values, as seen in Fig. 1. However, first rather than plotting observations by their exact positions on the celestial sphere (which would not be particularly insightful), we show how a given property changes as a function of RA. We have used this variable as a proxy for time in a series of heliocentric velocities for individual galaxies, treating the 0–24 h range of RA analogously to a 24-h time period, but now in the J2000 galactic frame of reference. This plot created using a right ascension (celestial equivalent of longitude) variable is commonly constructed in the context of observational astronomy when tracking the position of celestial objects over time. In this approach, the regular rotation of the Earth is used to map RA values onto observational time.

In this way, Fig. 3 displays differences of successive 2^m-step averages of large-scale fluctuations over a given scale in the receding redshifted speeds $\Delta_{2^m} V_H$ (in km s^{-1}) for $m = 5, \ldots, 12$, as originally proposed for the heliospheric plasma by Burlaga (1993),[36] compare Sec. 9.4.2 and Fig. 9.7 in his monograph.[35] Naturally, the clustering of galaxies occurs at scales vastly different from those in the Solar System. Nevertheless, both systems with hierarchical clustering exhibit intermittent spatial or temporal fluctuations. Those are generic signatures of systems governed by scale-free, nonlinear dynamics. We recognize, however, that a similar multifractal spectrum does not necessarily imply a direct physical connection between these systems.

In our view, both systems self-organize through scale-invariant processes. Therefore, one can identify patterns or trends, which may correspond to certain celestial regions or astronomical phenomena. Moreover, any deviations from the ideal linear Hubble law can provide insights into large-scale structures, peculiar motions, and evolutionary effects. In particular, we observe some irregular bursty, spiky, inhomogeneous (aperiodic and asymmetric) features of varying widths, which are characteristic for multifractal fluctuations in intermittent turbulence. In most cases, the magnitudes of positive fluctuations are somewhat greater than those for the negative fluctuations. Because time series for larger scales appear as magnified parts of the time series for the velocity increments on smaller scales, it seems that the cosmological fluctuations are self-affine across different scales. Hence, we can proceed with the multifractal analysis for various q values and scales $l := L_H$ described in Sec. II, Eq. (1). The probability measures $p(l)$ as a function of scale l (normalized) are now constructed according to Eq. (12) for each category, as obtained using the *UZCAT* galaxy catalog data shown in Fig. 1.

Next, in Figs. 4 and 5, both average logarithmic probability $\langle \log_{10} p_i(l)\rangle$ and pseudoprobability $\langle \log_{10} \mu_i(q, l)\rangle$ measures vs $\log_{10} l$ for all colored categories in the *UZCAT* catalog are now presented for the following (positive and negative) values of various q (Values of q yielding very robust fittings with $R^2 < 0.975$ and $r < 0.975$ have been rejected, where r denotes the Pearson correlation coefficient). As we see, the calculated slopes can be fitted to linear functions over a range of scales spanning typically four to even five orders of magnitude. Hence, similarly to the case of the heliospheric plasma, cf., 12, 13, and 28, we can obtain the multifractal spectrum using *UZCAT* data and compare the observational points with the weighted one-scale or the two-scale Cantor set models, as discussed in Sec. III B.

The generalized dimensions D_q as a function of q and the universal singularity spectrum $f(\alpha)$ as a function of singularity strength α are shown in Figs. 6 and 7, respectively. The values of D_q and $f(\alpha)$, as computed from Eqs. (5) and (6), obtained using the *UZCAT* data (denoted by boxes) and compared with both Cantor set models, cf. Fig. 3 of Ref. 33. As expected, D_q decreases with increasing q, consistent with Fig. 9.1 (a) of Ref. 14. In particular, we recover the capacity $f(\alpha_0) := D_0 = 1.0$ and the information dimensions $D_1 \lesssim 1.0$ for the 1-D proxy of the 3D space occupied by galaxies. The empirical values are in good agreement with the theoretical weighted Cantor set models.[2]

To select correctly the model parameters (p_1, p_2, l_1, l_2), we have used the Huber loss metric,[37] which combines the MSE and MAE metrics, to provide a loss function less sensitive to outliers, e.g., due to irregular intervals in the time series. Furthermore, Akaike Information Criterion (AIC[38]) and Bayesian Information Criterion (BIC[39]) were used for model selection to identify the best statistical representation of the data set. For each model i, we calculated the difference $\delta_i = IC_i - IC_{\min}$, where IC_i is the information criterion score (AIC/BIC), and $\mathrm{IC}_{\min}$ is the minimum information criterion score among compared models. In all analyzed cases, $\delta_i > 10$, indicating evidence against the competing model, and confirming that

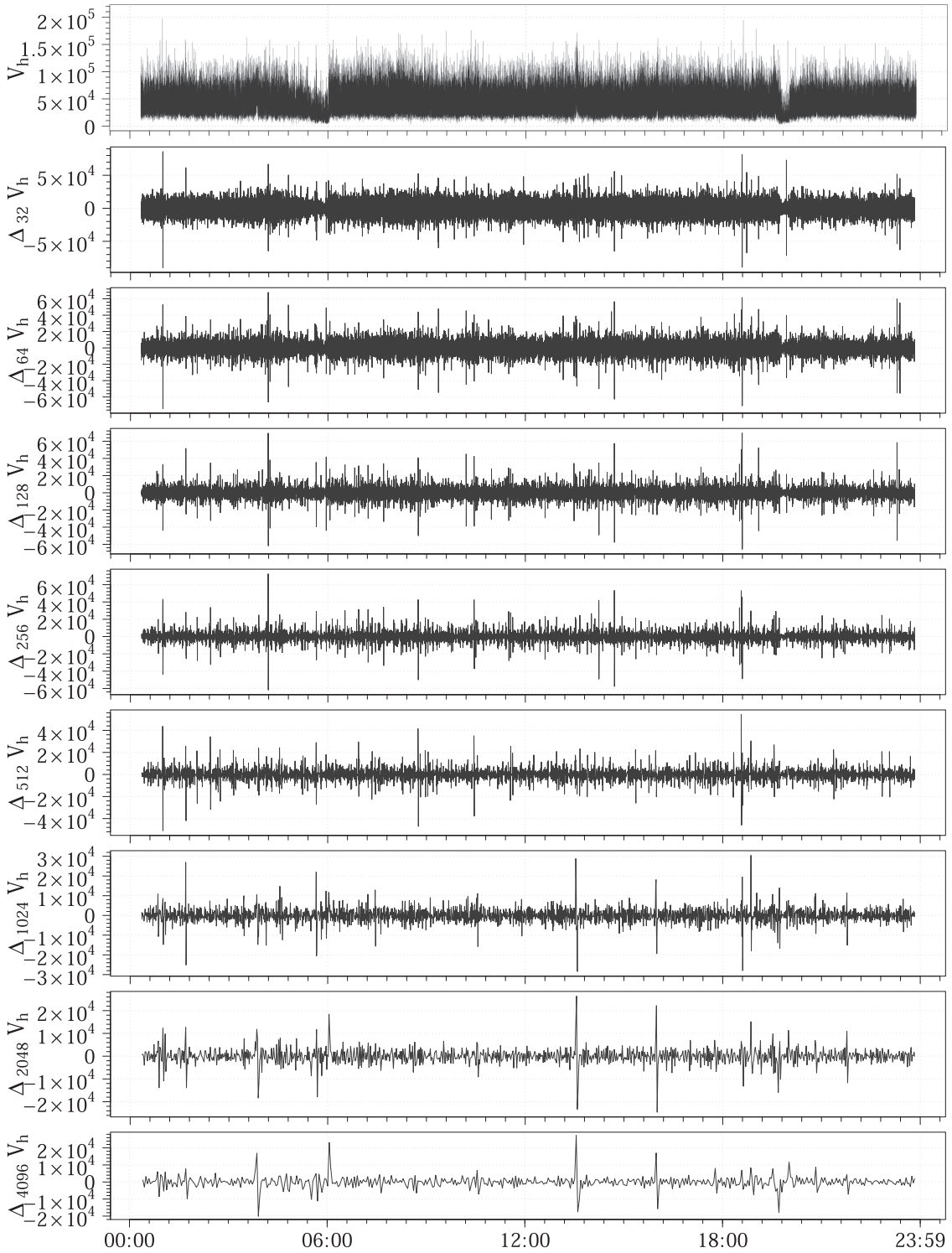

FIG. 3. The differences of successive 2^m-step averages $\Delta_{2^m} V_H$ [km s^{-1}] of large-scale speed fluctuations for $m = 5, \ldots, 12$ using observed distribution of galaxies based on the selected *UZCAT* data.

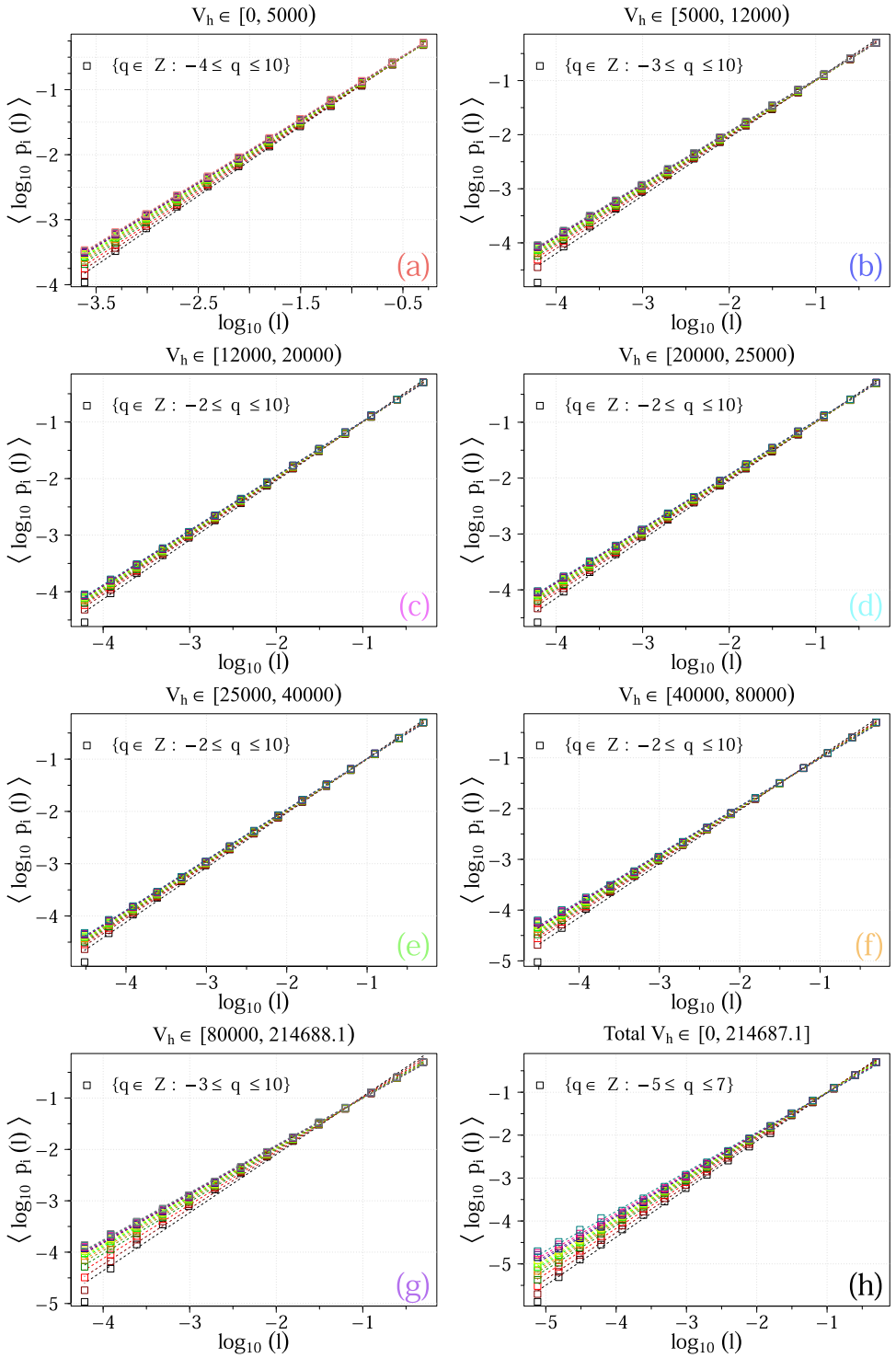

FIG. 4. Generalized average logarithmic probability $\langle \log_{10} p_i(l) \rangle$ depending on $\log_{10} l$ various q using the *UZCAT* catalog.

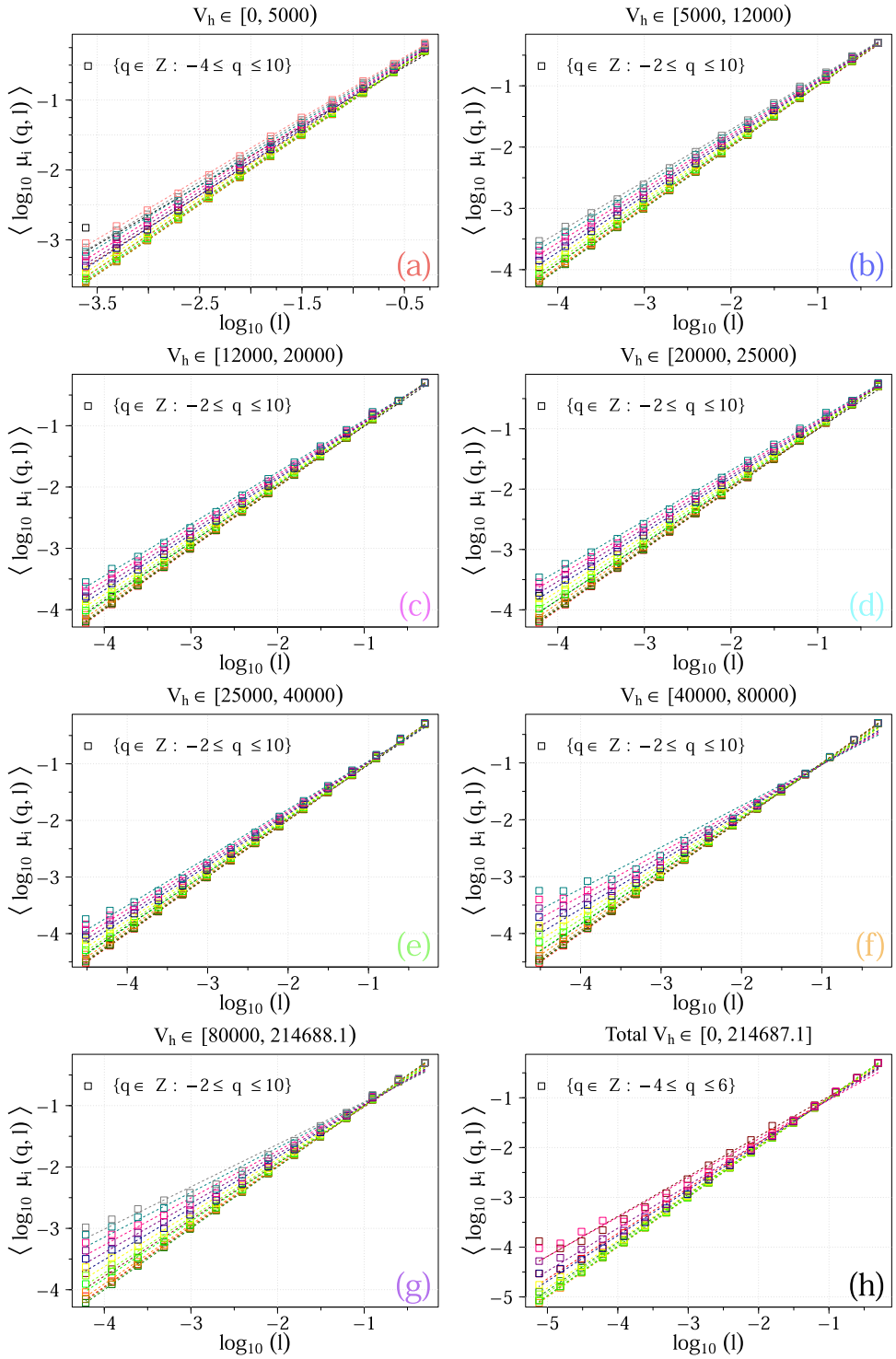

FIG. 5. Generalized average logarithmic pseudoprobability $\langle \log_{10} \mu_i(q, l) \rangle$ depending on $\log_{10} l$ for various q using the *UZCAT* catalog.

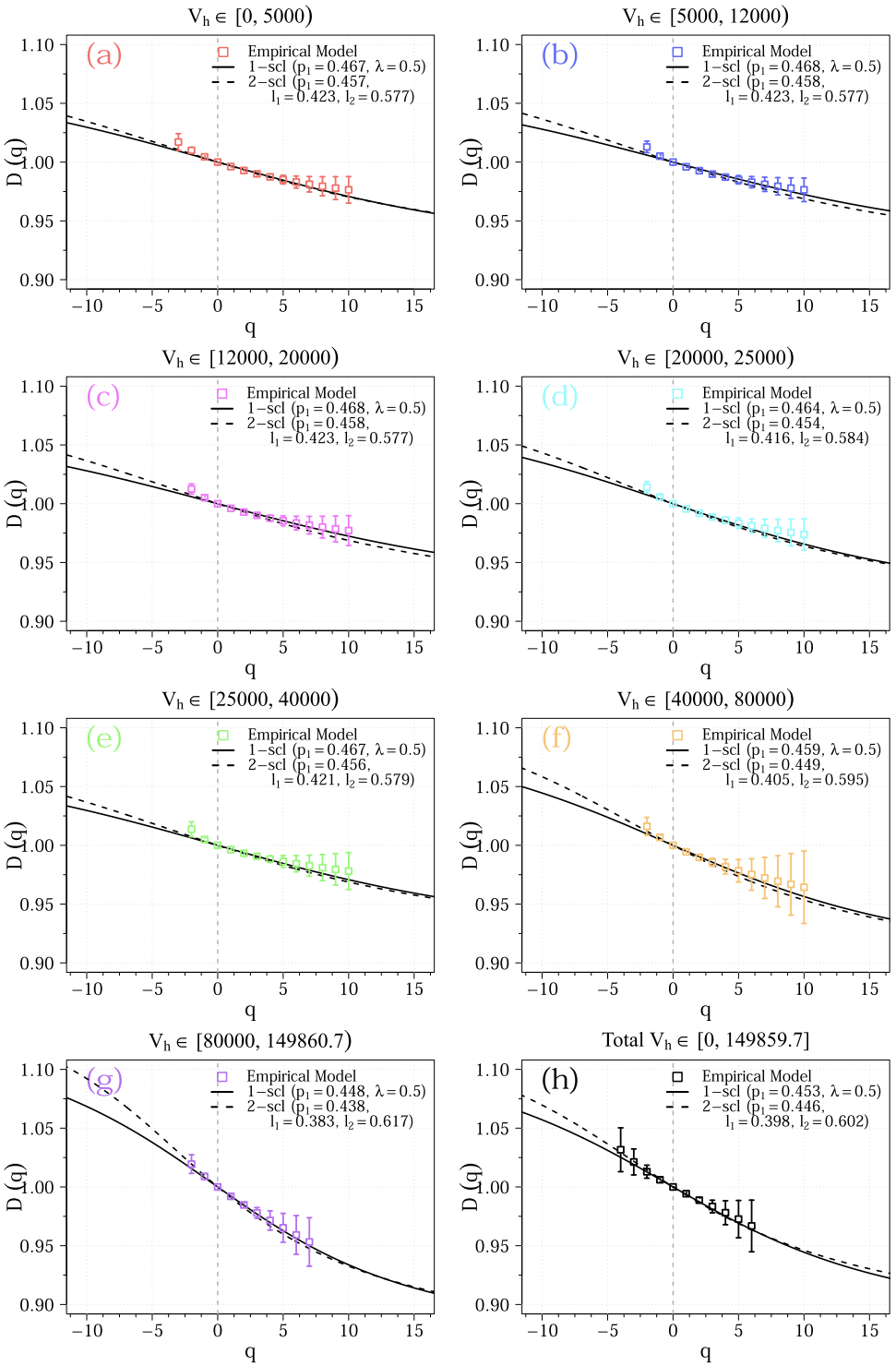

FIG. 6. The obtained generalized dimensions D_q as functions of q (colored boxes) for the observation categories of data in the *UZCAT* catalog (a)–(h) compared with the one-scale (continuous lines) or the two-scale (dashed lines) weighted Cantor models. The optimal model parameters are noted in the top right corner of each plot.

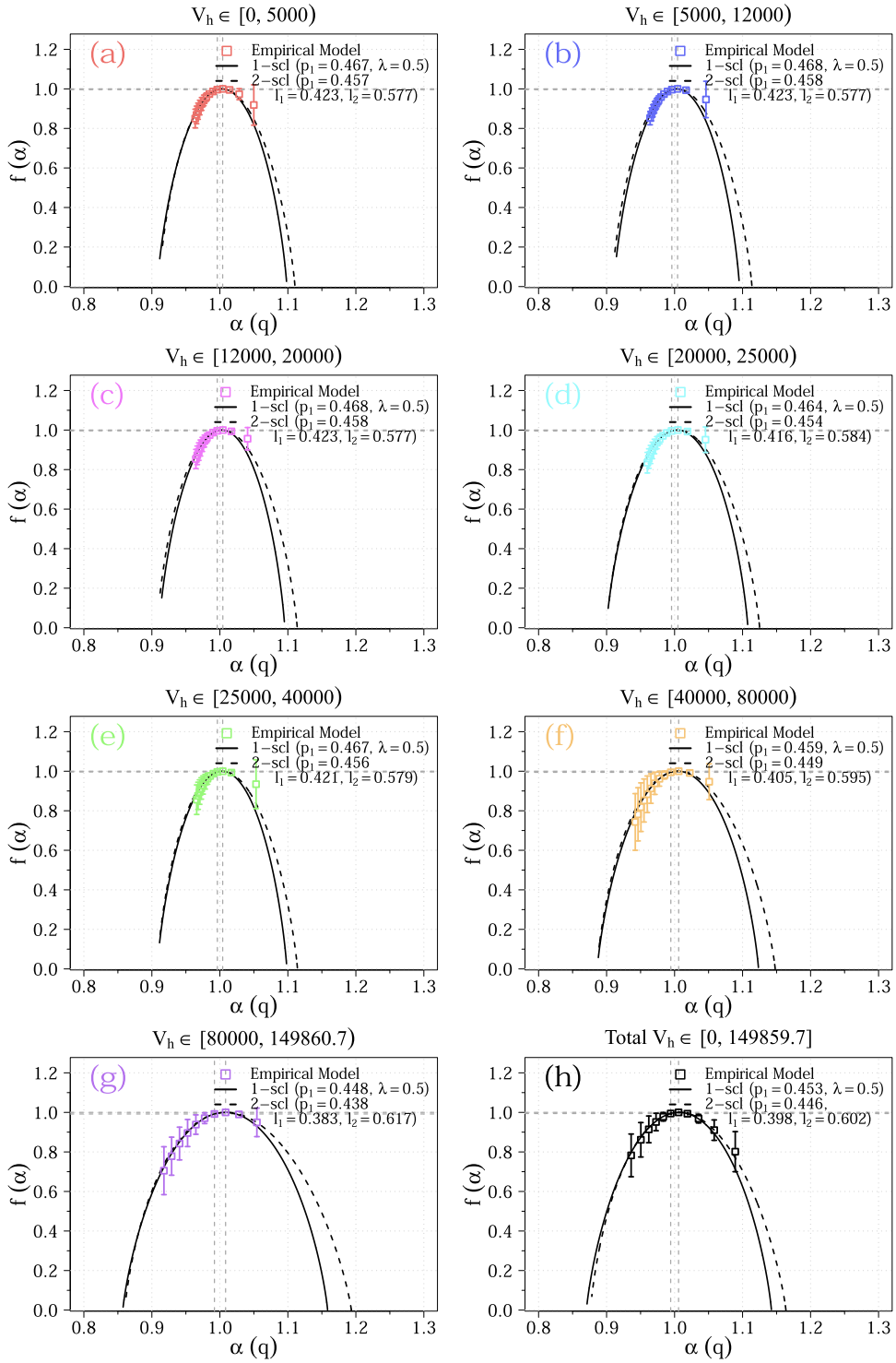

FIG. 7. The obtained multifractal measures of the multifractal spectrum $f(\alpha)$ as a function of the singularity strength α (colored boxes) for the various observation data of the *UZCAT* catalog (a)–(h) compared with the one-scale (continuous lines) or the two-scale (dashed lines) weighted Cantor models. The optimal model parameters are noted in the top right corner of each plot.

the two-scale model provides a better fit. However, because the simplest model is generally more convenient, it remains inconclusive whether both scales are strictly necessary. Further, for the two-scale Cantor model (as well as for the one-scale model), we have $p_1 + p_2 = 1$ (see also Fig. 3.9 of Ref. 2), so the fragmentation with probability $p_1 = p$ among length l_1 is effectively equivalent to the fragmentation with $p_2 = 1 - p$ under l_2.

Even though, we have not imposed the condition $l_1 = l_2 := \lambda = \frac{1}{2}$ for the one-scale nor $l_1 + l_2 = 1$ for the two-scale fits using Eq. (9), the catalogued observations are nevertheless reasonably consistent with the p-model or one-scale symmetric Cantor set spectrum (continuous lines), with $\lambda = 0.5$ and $p \approx 0.45$ (i.e., $p < \frac{1}{2}$). Naturally, a somewhat better agreement is observed with the asymmetric two-scale (dashed lines) Cantor set model, which incorporates parameter p and two different scales l_1 and l_2 into the theoretical model given by Eq. (9), while still satisfying the space-filling condition $l_1 + l_2 = 1$. Therefore, it is worth noting that multifractal behavior is possible, even when the entire supporting 3D space ($D_0 + 2$ with $D_0 = 1$) is filled with galaxies, but with varying probabilities. Only in the special case $p = \frac{1}{2}$ does multifractality disappear ($\Delta = 0$). Anyway, these values of 1D proxy are fitted to the theoretical solutions of Eq. (7), especially for $q > 0$ (left part of the spectrum, where more densely occupied fragments are magnified) and still somewhat less clearly for $q < 0$ (right side, where the galaxies occur with lower probability).

However, the degree of multifractality, which quantifies the deviation from a strictly monofractal behavior, $\Delta = 0.1 - 0.15$ is substantially smaller than that observed inside the heliosphere $\Delta = 0.3 - 0.7$, yet larger than in nonmultifractal ($\Delta \approx 0$) and relatively quiescent non-intermittent regions of the very local interstellar medium (VLISM) after Voyager 1 crossed the heliospheric boundaries (at ~122 AU) in 2012, see Ref. 13. These small values of Δ suggest fractal rather than multifractal behavior in the galaxy distribution. However, the number of the catalogued galaxies is much smaller than the estimated total number of galaxies in the entire Universe. Therefore, the ultimate answer as to whether the actual galaxy distribution is compatible with fractal or multifractal homogeneity must be deferred to future investigations. Meanwhile, the parameters $p \approx 0.45$ and $\lambda = \frac{1}{2}$ for the one-scale model appear to be related to the presence of voids in the large-scale distribution of matter. In particular, the calculated slightly asymmetric spectra with $A = 0.9 - 1.4$ for two-scale weighted Cantor set model ($A \neq 1$) could be related to the deviation from Hubble's law in a uniformly expanding Universe.

Therefore, we have also calculated the multifractal parameter Δ and asymmetry A, with their calculated respective standard deviations, using Eqs. (10) and (11) in the observed Universe as a function of distance for all the categories: red, blue, magenta, cyan, green, orange, and violet, which are provided in Table I. To calculate the standard deviations σ_Δ and σ_A for these parameters, we have used the bootstrapping method. This method works by repeatedly resampling the original time series (e.g., 100 times) with replacement and re-running the entire analysis for each resampled data set. By building a resulting distribution that yields 100 different estimates of the multifractality Δ and asymmetry A, we can then compute the standard deviations σ of these distributions to obtain the corresponding standard errors.

The obtained differences listed in Table I vary slightly (from 0.1 to 0.12) for nearby galaxies ($\Delta \simeq 0.09$) and for more distant galaxies ($\Delta \simeq 0.12$) receding from our Solar System. This variation should be attributed to differences in the population of receding galaxies across various categories according to their distances. In the violet subset, a somewhat higher multifractality parameter, $\Delta = 0.17$, follows from higher—but still moderate—relativistic redshifts, $z > 0.3$. However, we note that for ultra-relativistic speeds, corrections from general relativity should be considered, which could make the results somewhat dependent on the chosen cosmological model. The parameter $p \approx 0.45$ ($\lambda = \frac{1}{2}$) for the one-scale model is apparently related to the presence of voids in the large-scale distribution of matter. A possible asymmetry ($A \approx 0.8$) of the total spectrum for the two-scale weighted Cantor set ($A \neq 1$) could admittedly be attributed to deviations from Hubble's law for the ideally uniform expansion of the Universe.

V. CONCLUSIONS

Based on a sample consisting of various categories of about 800 000 galaxies taken from the *UZCAT* catalog, as highlighted by colors and letters in Fig. 1, for the large-scale distribution of all galaxies existing in the observable Universe, we have studied intermittent self-affine multifractal fluctuations in the average heliocentric (relativistic redshifted) velocities, as presented in Fig. 3.

Basically, using the calculated slopes depicted in Fig. 4 and the one-scale and two-scale weighted Cantor set models, we have ultimately obtained the generalized dimensions and the universal multifractal spectrum shown in Figs. 6 and 7. It is worth noting that the observed multifractal spectrum for lower redshifts does not very much depend on any specific model of general relativity or any particular scenario of the evolution of the Universe, but is based solely on direct and comprehensive analysis of redshifted distances from the best currently available catalog of observed galaxies. In this way, we have provided new supporting important evidence that the large-scale galaxy distribution most probably exhibits multifractal structure consistent with the weighted one- or two-scale Cantor set model. One may further speculate that the model parameters $p < \frac{1}{2}$ ($\lambda = \frac{1}{2}$) of Eq. (7) with Δ of Eq. (10) are apparently related to some voids in the large-scale distribution of matter in the Universe, assuming that these voids are not caused by dark matter.

Because of the differences in the populations of various classes of galaxies, the degree of multifractality Δ of the spectrum varies slightly between 0.09 and 0.12 for increasingly distant, receding regions, as listed in Table I. In particular, a somewhat higher value of 0.17 follows from higher, though still moderate relativistic, redshifts. A possible asymmetry $A \sim \frac{3}{4}$ of the total spectrum may result from the deviations from the ideal Hubble's law. However, the degree of multifractality is rather small, $\Delta \lesssim 0.2$, as obtained for admittedly only a tiny fraction of all possibly existing galaxies. Hence, one is still not able to give any definitive answer whether the galaxies in the entire Universe should actually exhibit multifractal or even a simple fractal distribution, as has already been suggested in Ref. 1.

On the occasion of the hundredth anniversary of the discovery of the first galaxy beyond the Milky Way, however, we are still hoping for the discovery of fractal scaling laws for galaxies may be a

valuable addition to the ultimate explanations of the distribution of matter in the Universe.

ACKNOWLEDGMENTS

We thank Vincenzo Carbone (1957–2025) from the University of Calabria and Len F. Burlga from the NASA Goddard Space flight Center for help in methods of fractal analysis. The influential contribution of John Huchra (1948–2010) to the galaxy catalog should be acknowledged. We would like to thank the reviewers for their inspiring comments, which greatly improved our presentation. The sky map of the selected galaxies has been constructed using the *AstroPy* package for Astronomy in Python. The data have been processed using statistical programming language R. This work has been supported by the National Science Centre, Poland (Narodowe Centrum Nauki) through Grant No. 2021/41/B/ST10/00823.

AUTHOR DECLARATIONS

Conflict of Interest

The authors have no conflicts to disclose.

Author Contributions

Following the previous work by Macek *et al.* (2014), see Ref. 13, W.M.M. wrote the main manuscript and D.W. performed the numerical calculations, prepared the figures, and contributed to the paper.

W. M. Macek: Conceptualization (lead); Methodology (equal); Supervision (equal); Writing – original draft (lead). **D. Wójcik:** Data curation (equal); Software (equal); Writing – original draft (supporting).

DATA AVAILABILITY

The data that support the findings of this study are available through the Smithsonian Astronomical Observatory Telescope Data Center at http://tdc-www.harvard.edu/zcat/velocity.dat, Ref. 40; the CfA Redshift (Z)CATalog UZCAT at http://tdc-www.harvard.edu/zcat/zcom.htm, Ref. 41; and Zenodo at https://zenodo.org/records/18304542, Ref. 42.

REFERENCES

[1]B. B. Mandelbrot, *The Fractal Geometry of Nature* (Freeman, New York, 1982).
[2]W. M. Macek, *The Origin of the World: Cosmos or Chaos?* [Cardinal Stefan Wyszyński University (UKSW) Scientific Editions, Warsaw, Poland, 2020] in English, ISBN: 978-83-8090-686-0, e-ISBN: 978-83-8090-687-7, available at https://wydawnictwo.uksw.edu.pl/ksiegarnia/886–e-book-the-origin-of-the-world-cosmos-or-chaos.html
[3]W. M. Macek, in *14th Chaotic Modeling and Simulation International Conference*, edited by C. H. Skiadas and Y. Dirtballs (Springer International Publishing, Cham, 2022), pp. 311–326, available at https://link.springer.com/chapter/10.1007/978-3-030-96964-6_21
[4]J. Maddox, Nature **329**, 195 (1987).
[5]S. Teles, A. Lopes, and M. B. Ribeiro, Eur. Phys. J. C **82**, 896 (2022).
[6]B. L. Dias, F. Avila, and A. Bernui, Mon. Not. R. Astronom. Soc. **526**, 3219 (2023).
[7]B. J. T. Jones, V. J. Martinez, E. Saar, and J. Einasto, Astrophys. J. Lett. **332**, L1 (1988).
[8]J. Gaite, Adv. Astron. **2021**, 6680938.
[9]B. J. Jones, V. J. Martínez, E. Saar, and V. Trimble, Rev. Mod. Phys. **76**, 1211 (2005).
[10]L. Burlaga, Nonlinear Process. Geophys. **11**, 441 (2004).
[11]W. M. Macek, A. Wawrzaszek, and V. Carbone, Geophys. Res. Lett. **38**, L19103 (2011).
[12]W. M. Macek, A. Wawrzaszek, and V. Carbone, J. Geophys. Res. **117**, A12101, https://doi.org/10.1029/2012JA018129 (2012).
[13]W. M. Macek, A. Wawrzaszek, and L. F. Burlaga, Astrophys. J. Lett. **793**, L30 (2014).
[14]E. Ott, *Chaos in Dynamical Systems* (Cambridge University Press, Cambridge, 1993).
[15]J. P. Huchra, L. M. Macri, K. L. Masters, T. H. Jarrett, P. Berlind, M. Calkins, A. C. Crook, R. Cutri, P. Erdoğdu, E. Falco, T. George, C. M. Hutcheson, O. Lahav, J. Mader, J. D. Mink, N. Martimbeau, S. Schneider, M. Skrutskie, S. Tokarz, and M. Westover, Astrophys. J. Suppl. Ser. **199**, 26 (2012).
[16]W. M. Macek, in *18th International Conference on Non Linear Analysis and Modeling: Theory and Applications, Plenary Lecture* (Springer, 2025), available at http://www.cmsim.org/chaos2025.html.
[17]W. M. Macek and D. Wójcik, AGU Annual Meeting **NG13A**, 1520274 (2024), available at https://agu.confex.com/agu/agu25/meetingapp.cgi/; presentation available at https://essopenarchive.org/users/865706/articles/1246542-multifractal-spectrum-observed-in-the-distribution-of-galaxies?commit=f99bf2cfaebe81fa28f8018da77384cb14bf0610.
[18]V. J. Martinez, B. J. T. Jones, R. Dominguez-Tenreiro, and R. van de Weygaert, Astrophys. J. Lett. **357**, 50 (1990).
[19]S. A. Shectman, S. D. Landy, A. Oemler, D. L. Tucker, H. Lin, R. P. Kirshner, and P. L. Schechter, Astrophys. J. Lett. **470**, 172 (1996).
[20]M. F. Skrutskie, R. M. Cutri, R. Stiening, M. D. Weinberg, S. Schneider, J. M. Carpenter, C. Beichman, R. Capps, T. Chester, J. Elias, J. Huchra, J. Liebert, C. Lonsdale, D. G. Monet, S. Price, P. Seitzer, T. Jarrett, J. D. Kirkpatrick, J. E. Gizis, E. Howard, T. Evans, J. Fowler, L. Fullmer, R. Hurt, R. Light, E. L. Kopan, K. A. Marsh, H. L. McCallon, R. Tam, S. Van Dyk, and S. Wheelock, Astrophys. J. **131**, 1163 (2006), available at https://iopscience.iop.org/article/10.1086/498708.
[21]D. H. Jones, M. A. Read, W. Saunders, M. Colless, T. Jarrett, Q. A. Parker, A. P. Fairall, T. Mauch, E. M. Sadler, F. G. Watson, D. Burton, L. A. Campbell, P. Cass, S. M. Croom, J. Dawe, K. Fiegert, L. Frankcombe, M. Hartley, J. Huchra, D. James, E. Kirby, O. Lahav, J. Lucey, G. A. Mamon, L. Moore, B. A. Peterson, S. Prior, D. Proust, K. Russell, V. Safouris, K.-I. Wakamatsu, E. Westra, and M. Williams, Mon. Not. R. Astron. Soc. **399**, 683 (2009).
[22]T. M. Davis and C. H. Lineweaver, Publ. Astron. Soc. Aust. **21**, 97 (2004).
[23]P. Antonyuk, J. Phys.: Conf. Ser. **1557**, 012039 (2020).
[24]D. G. York, J. Adelman, J. John E. Anderson, S. F. Anderson, J. Annis, N. A. Bahcall, J. A. Bakken, R. Barkhouser, S. Bastian, E. Berman, W. N. Boroski, S. Bracker, C. Briegel, J. W. Briggs, J. Brinkmann, R. Brunner, S. Burles, L. Carey, M. A. Carr, F. J. Castander, B. Chen, P. L. Colestock, A. J. Connolly, J. H. Crocker, I. Csabai, P. C. Czarapata, J. E. Davis, M. Doi, T. Dombeck, D. Eisenstein, N. Ellman, B. R. Elms, M. L. Evans, X. Fan, G. R. Federwitz, L. Fiscelli, S. Friedman, J. A. Frieman, M. Fukugita, B. Gillespie, J. E. Gunn, V. K. Gurbani, E. de Haas, M. Haldeman, F. H. Harris, J. Hayes, T. M. Heckman, G. S. Hennessy, R. B. Hindsley, S. Holm, D. J. Holmgren, C. hao Huang, C. Hull, D. Husby, S.-I. Ichikawa, T. Ichikawa, Ž. Ivezić, S. Kent, R. S. J. Kim, E. Kinney, M. Klaene, A. N. Kleinman, S. Kleinman, G. R. Knapp, J. Korienek, R. G. Kron, P. Z. Kunszt, D. Q. Lamb, B. Lee, R. F. Leger, S. Limmongkol, C. Lindenmeyer, D. C. Long, C. Loomis, J. Loveday, R. Lucinio, R. H. Lupton, B. MacKinnon, E. J. Mannery, P. M. Mantsch, B. Margon, P. McGehee, T. A. McKay, A. Meiksin, A. Merelli, D. G. Monet, J. A. Munn, V. K. Narayanan, T. Nash, E. Neilsen, R. Neswold, H. J. Newberg, R. C. Nichol, T. Nicinski, M. Nonino, N. Okada, S. Okamura, J. P. Ostriker, R. Owen, A. G. Pauls, J. Peoples, R. L. Peterson, D. Petravick, J. R. Pier, A. Pope, R. Pordes, A. Prosapio, R. Rechenmacher, T. R. Quinn, G. T. Richards, M. W. Richmond, C. H. Rivetta, C. M. Rockosi, K. Ruthmansdorfer, D. Sandford, D. J. Schlegel, D. P. Schneider, M. Sekiguchi, G. Sergey, K. Shimasaku, W. A. Siegmund, S. Smee, J. A. Smith, S. Snedden, R. Stone, C. Stoughton, M. A. Strauss, C. Stubbs, M. SubbaRao, A. S. Szalay, I. Szapudi, G. P. Szokoly, A. R. Thakar, C. Tremonti, D. L. Tucker, A. Uomoto, D. V. Berk, M. S. Vogeley, P. Waddell, S. I. Wang, M. Watanabe, D. H. Weinberg, B. Yanny, and N. Yasuda, Astron. J. **120**, 1579 (2000).
[25]A. Dressler, Astrophys. J. Supp. Ser. **42**, 565 (1980).

[26]K. Falconer, *Fractal Geometry: Mathematical Foundations and Applications* (Wiley, New York, 1990).
[27]S. H. Strogatz, *Nonlinear Dynamics and Chaos: With Applications to Physics, Biology, Chemistry, and Engineering*, Library (Addison-Wesley, Reading, Massachusetts, 1994), pp. 512.
[28]W. M. Macek and A. Wawrzaszek, J. Geophys. Res. **114**, A03108, https://doi.org/10.1029/2008JA013795 (2009).
[29]U. Frisch, *Turbulence. The Legacy of A.N. Kolmogorov* (Cambridge University Press, Cambridge UK, 1995).
[30]D. Biskamp, *Magnetohydrodynamic Turbulence* (Cambridge University Press, Cambridge, UK, 2003).
[31]A. Chhabra and R. V. Jensen, Phys. Rev. Lett. **62**, 1327 (1989).
[32]A. B. Chhabra, C. Meneveau, R. V. Jensen, and K. R. Sreenivasan, Phys. Rev. A **40**, 5284 (1989).
[33]W. M. Macek, Nonlinear Process. Geophys. **14**, 695 (2007).
[34]C. Meneveau and K. R. Sreenivasan, Phys. Rev. Lett. **59**, 1424 (1987).
[35]L. F. Burlaga, *Interplanetary Magnetohydrodynamics* (Oxford University Press, New York, 1995).
[36]L. F. Burlaga, "Intermittent turbulence in large-scale velocity fluctuations at 1 AU near solar maximum," J. Geophys. Res. Space Phys. **98**, 17467–17473, https://doi.org/10.1029/93JA01630 (1993).
[37]P. J. Huber, Ann. Math. Stat. **35**, 73 (1964).
[38]H. Akaike, IEEE Trans. Audio Electroacoust. Control **19**, 716 (1974).
[39]G. Schwarz, Ann. Stat. **6**, 461 (1978).
[40]Smithsonian Astronomical Observatory Telescope Data Center (2025). Dataset. http://tdc-www.harvard.edu/zcat/velocity.dat
[41]CfA Redshift (Z)CATalog UZCAT (2008). Dataset. http://tdc-www.harvard.edu/zcat/zcom.htm
[42]D. Wójcik and W. M. Macek (2026). "Multifractal spectrum observed in the Universe distribution of galaxies - Dataset," Zenodo. https://zenodo.org/records/18304542